JOURNAL OF VIROLOGY, June 2009, p. 5544–5555 Vol. 83, No. 11
0022-538X/09/$08.00+0 doi:10.1128/JVI.02673-08

Major Histocompatibility Complex Haplotype Determines hsp70-Dependent Protection against Measles Virus Neurovirulence▽

Thomas Carsillo,[1,2] Mary Carsillo,[1,2] Zachary Traylor,[1] Päivi Rajala-Schultz,[3] Phillip Popovich,[4] Stefan Niewiesk,[1,2,4] and Michael Oglesbee[1,4]*

Department of Veterinary Biosciences,[1] Center for Microbial Interface Biology,[2] Department of Veterinary Preventive Medicine,[3] and Department of Molecular Virology, Immunology and Medical Genetics,[4] the Ohio State University, Columbus, Ohio 43210

Received 29 December 2008/Accepted 20 March 2009

In vitro studies show that hsp70 promotes gene expression for multiple viral families, although there are few reports on the in vivo significance of virus-hsp70 interaction. Previously we showed that hsp70-dependent stimulation of Edmonston measles virus (Ed MeV) transcription caused an increased cytopathic effect and mortality in transgenic hsp70-overexpressing C57BL/6 mice (*H-2^b*). The response to MeV infection is influenced by the major histocompatibility complex haplotype; *H-2^d* mice are resistant to brain infection due to robust antiviral immune responses, whereas *H-2^b* mice are susceptible due to deficiencies in this response. We therefore tested the hypothesis that the outcome of MeV-hsp70 interaction may be dependent upon the host *H-2* haplotype. The impact of selective neuronal hsp70 overexpression on Ed MeV brain infection was tested with congenic C57BL/10 *H-2^d* neonatal mice. In this context, hsp70 overexpression conferred complete protection against virus-induced mortality, compared to >30% mortality in nontransgenic mice. Selective depletion of T-cell populations showed that transgenic mice exhibit a diminished reliance on T cells for protection. Brain transcript analysis indicated enhanced innate immune activation and signaling through Toll-like receptors 2 and 4 at early times postinfection for transgenic infected mice relative to those for nontransgenic infected mice. Collectively, results suggest that hsp70 can enhance innate antiviral immunity through Toll-like receptor signaling, supporting a protective role for physiological responses that enhance tissue levels of hsp70 (e.g., fever), and that the *H-2* haplotype determines the effectiveness of this response.

The cellular stress response is characterized in part by the increased expression of heat shock proteins, particularly the major inducible 70-kDa isoform (hsp70, also known as hsp72). Numerous physiological stimuli can increase cellular levels of hsp70, including febrile temperatures that frequently accompany viral infection, and 70-kDa heat shock proteins support replication of both DNA and RNA viruses (reviewed in references 30 and 37), yet there is a paucity of studies examining the impact of elevated heat shock protein expression on the outcome of viral infection within animals.

In vitro studies have shown that elevated cellular levels of hsp70 are associated with increased gene expression of the morbilliviruses measles virus (MeV) and canine distemper virus, members of the *Paramyxoviridae*. Selective overexpression via stable transfection or induction via transient heat shock both stimulate viral transcription and genome replication, resulting in increased viral protein expression and cytopathic effect (CPE) (9, 38, 39, 52, 53). hsp70-dependent gene expression reflects direct interaction between hsp70 and the viral nucleocapsid, which is composed of the single-stranded negative-sense genomic RNA packaged by the nucleocapsid protein (N) (40, 52, 53). The N-protein C terminus provides docking sites for both the viral polymerase and hsp70 (reviewed in reference 4). For the Edmonston B strain of MeV (Ed MeV), one of these docking sites (N-protein amino acids 517 to 525, also known as Box-3) has been shown to specifically support hsp70-dependent transcription. A single amino acid substitution within Box-3 (N522D) disrupts binding of hsp70 to Box-3, and recombinant infectious Ed MeV incorporating the N522D mutation (Ed N-522D) exhibits an attenuated transcriptional response to hsp70 without hsp70-dependent increases in genome levels being affected (9, 57, 58).

The mouse model of MeV brain infection was previously used to show that interaction between Ed MeV and hsp70 can enhance viral virulence (8). Transgenic (TG) C57BL/6 mice were generated that overexpress hsp70 in neurons, which are the target of MeV brain infection. The expression construct utilized a neuron-specific enolase promoter, and neuronal expression of the *hsp70* transgene was confirmed by immunohistochemisty. Intracranial inoculation of neonatal hsp70-overexpressing mice with Ed MeV resulted in a 100-fold increase in the brain viral RNA burden, increased viral antigen expression and CPE, and a 5-fold increase in virus-induced mortality relative to that for nontransgenic (NT) mice. Mice challenged with the Ed N-522D variant exhibited no difference in mortality or brain viral RNA levels between the TG and NT groups, proof that it was the viral transcriptional response to hsp70 that was the basis for the observed differences in infection outcome.

Susceptibility and resistance to MeV-induced encephalitis in the mouse are determined by the *H-2* haplotype, major histocompatibility complex (MHC) class I, II, and III loci that dictate the effectiveness of immune responses to MeV infection (35, 36, 55). Mice carrying the *H-2^b* or *H-2^k* allele (e.g., the C57BL/6 and C3H strains, respectively) are susceptible to in-

* Corresponding author. Mailing address: Department of Veterinary Biosciences, The Ohio State University, 1925 Coffey Road, Columbus, OH 43210. Phone: (614) 292-9672. Fax: (614) 292-6473. E-mail: oglesbee.1@osu.edu.

▽ Published ahead of print on 25 March 2009.

tracranial MeV infection, and this susceptibility has been attributed to an inefficient $CD4^+$ T-cell response and the associated release of gamma interferon (IFN-γ), the latter directly mediating noncytolytic viral clearance from neurons (14, 15, 44, 55). In contrast, mice carrying the *H-2*^{d} allele (e.g., BALB/c) generate an efficient T-cell response, resulting in robust IFN-γ production and protection from clinically significant MeV brain infection.

The current work tested the hypothesis that TG hsp70 overexpression in neurons, in the context of the *H-2*^{d} allele, may be host protective. When hsp70 is overexpressed in neural tissue of C57BL/6 mice, the inefficient T-cell response associated with the *H-2*^{b} allele combined with hsp70-dependent increases in viral gene expression leads to enhanced CPE and mortality (8). But when that same hsp70-dependent stimulation of MeV gene expression occurs in the context of the *H-2*^{d} haplotype, there may be enhanced antiviral immune responses that result in host protection. Protection could reflect immune-stimulatory effects associated with increased levels of viral antigen and/or CPEs, in addition to direct innate immune stimulation by hsp70 that is released from virus-infected cells (32, 41). The hypothesis is supported by work showing that heat shock-induced elevation of hsp70 in brains of neonatal BALB/c (*H-2*^{d}) mice prior to infection results in enhanced viral clearance following subsequent intracranial inoculation with Ed MeV (7). Lacking is an understanding of how the mouse genetic background (i.e., differences in addition to the *H-2* haplotype) may have influenced these results, the effect of selective hsp70 overexpression versus that of the multiple heat shock protein family members that are induced following transient hyperthermia, and the contribution of the viral transcriptional response to hsp70 in determining the outcome of infection.

In order to determine the effect of the *H-2* haplotype on the hsp70-dependent outcome of MeV brain infection in neonatal mice, we placed the *hsp70* transgene in C57BL/6 *H-2*^{b} mice on an *H-2*^{d} background through crossbreeding with congenic C57BL/10 *H-2*^{d} mice. Intracranial inoculation with the Ed N-522D variant was used to determine the significance of hsp70-dependent viral transcription for the infection outcomes, since levels of viral gene expression can affect both CPE and antiviral immune responses to infection. Infection outcomes were quantified based upon virus-induced mortality, which, in turn, was related to the brain viral RNA burden and CPE.

MATERIALS AND METHODS

Generation of hsp70-TG *H-2*^{d} mice. Characterization of TG mice overexpressing human hsp70 under the control of the neuron-specific enolase promoter [C57BL/6-TgNSE(VSV/Hsp70)5769OGL] has been described previously (8). Congenic C57BL/10 mice carrying the *H-2*^{d} haplotype (C57BL/10.D2/NO1aHsd) were obtained from Harlan, United Kingdom. C57BL/10 and C57BL/6 mice differ by only three genetic loci, and C57BL/10.D2-TgNSE(VSV/Hsp70)5769OGL mice carrying the *H-2*^{d} haplotype were generated by back-crossing C57BL/6-TgNSE(VSV/Hsp70)5769OGL mice with C57BL/10.D2/NO1aHsd mice for two generations. Peripheral blood mononuclear cells (PBMCs), isolated from whole blood, were used to monitor the H-2 complex by flow cytometry using monoclonal antibodies specific for $H\text{-}2^b$ (AF6-88.5, fluorescein isothiocyanate (FITC)-conjugated; BD Pharmingen) and $H\text{-}2^d$ (SF1-1.1, R-PE-conjugated, BD Pharmingen) alloantigens. The content and expression of the hsp70 construct were confirmed by PCR and Southern blot analysis of genomic DNA and reverse transcriptase PCR (RT-PCR) analysis of total cell RNA as described previously (8). Mice were maintained as homozygotes for the *H-2*^{d} allele and the *hsp70* transgene.

Characterization of infected mice. Male and female TG and NT neonatal mice (42 h of age) were inoculated intracranially in the left cerebral hemisphere with Ed MeV or Ed N-522D MeV in a total volume of 10 μl as described previously (7, 8). Control mice received either 1× phosphate-buffered saline or an equivalent dose of virus that was irradiated with 6×10^4 μJ of short-wave UV light. All dams were primiparous. For survival analyses, mice were euthanized and brains harvested at 28 days postinfection (p.i.) or when animals met early-removal criteria (i.e., weight of <30 to 50% of the mean litter body weight, dehydration, and seizure activity). Five and ten days p.i. were also used as experimental end points for the analysis of innate immune responses by real-time RT-PCR of total brain RNA and to identify the time at which inflammatory cell infiltrates occur in tissue sections. Brains were sagittally sectioned. The right half of the brain was processed for total RNA isolation using the RNeasy lipid tissue mini kit (Qiagen). The left half of the brain was processed for light microscopic analysis of formalin-fixed paraffin-embedded tissue sections (14 to 28 days p.i.) or frozen sections (5 and 10 days p.i.).

Levels of viral RNA in total brain RNA were quantified by SYBR green real-time RT-PCR as described previously (7, 8). Levels of CD68, MHC II, Toll-like receptor 2 (TLR2), TLR4, and IFN-γ transcripts in total brain RNA were also quantified by SYBR green real-time RT-PCR as described previously by our group (20, 27), representing markers of innate immune activation (CD68 and MHC II), pathways for innate immune activation (TLR2 and TLR4), and a proinflammatory cytokine response known to mediate MeV clearance (IFN-γ).

Tissue sections were evaluated for CPE following routine hematoxylin-and-eosin (H&E) staining. Coronal sections at the level of +1.0 and −2.0 bregma (i.e., positions relative to the anatomical structure on the skull where the frontal and sagittal sutures meet) and midline sagittal sections of the metencephalon were evaluated. Descriptions of pathological changes pertain to the transverse sections at −2.0 bregma because of the inclusion of the hippocampus, a structure whose involvement in virus-induced CPE was an indicator of mortality. Histological evaluation was carried out with all samples when possible, although sample quality was occasionally compromised in cases of acute mortality. In the latter instances, all brain tissues were frozen for subsequent RNA isolation, forgoing the histological analyses.

Neurons were identified based upon their unique cell morphology as shown by H&E staining (i.e., soma containing basophilic Nissl substance and round nuclear profile with prominent nucleolus) and the lineage confirmed based upon NeuN immunohistochemical staining. Dead cells were identified as being of neuronal origin based upon the progression from degeneration (where the cell type could be identified) to cell death that was illustrated in tissues during the acute phase of infection. Neuronal death is characterized by hypereosinophilia and margination of a pyknotic or rhectic nucleus. Immunoreactivity for activated caspase 3 was used to distinguish between apoptotic and necrotic cell death.

CD3 immunohistochemical staining was used to confirm the identity of infiltrating lymphocytes as being of T-cell origin in formalin-fixed tissues. CD4 and CD8 immunohistochemical staining was performed on frozen sections from brains harvested at 5 or 10 days p.i. Glial fibrillary acidic protein (GFAP) immunohistochemistry was used to evaluate the degree of astrocytic reactivity in areas of gliosis. Finally, von Kossa histochemical staining was used to highlight areas of tissue mineralization. All histochemical and immunohistochemical staining procedures are routine procedures performed by the Comparative Pathology and Mouse Phenotyping Shared Resource, Department of Veterinary Biosciences and the Comprehensive Cancer Center, The Ohio State University. Tissues were evaluated in a blinded manner by a board-certified veterinary anatomical pathologist.

Depletion of $CD4^+$ and $CD8^+$ T cells. Hybridomas specific for mouse CD4 and mouse CD8 (GK1.5 and 2.43, respectively) were obtained from American Type Culture Collection and grown in advanced RPMI 1640–10% fetal calf serum–10 mM HEPES to a concentration of 4 mg/ml using a miniPERM bioreactor (Greiner Bio-One). The depletion protocol employed an initial subcutaneous injection of monoclonal antibody against CD4 and/or CD8 at 48 h of age, corresponding to the time at which infections are performed. Antibody administration was performed twice weekly and changed from subcutaneous to intraperitoneal injection at week two. For $CD4^+$ and $CD8^+$ combined T-cell depletion, the GK1.5 and 2.43 monoclonal antibodies were mixed in equal parts and the total volume was reduced by half using an Amicon Ultra-100K normal-molecular-weight-limit centrifugal filter device (Millipore). Binding and specificity of the monoclonal antibodies were not affected by the concentration. Previous experiments have shown that injection of isotype-matched monoclonal antibodies of unrelated specificities does not influence the $CD4^+$ and $CD8^+$ T-cell subsets (15). The effectiveness of in vivo depletion of T-cell subsets in

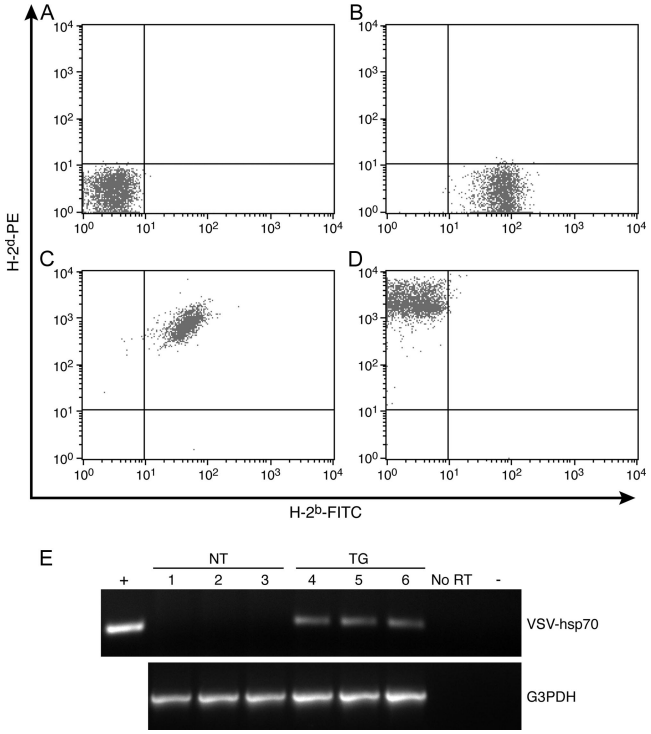

FIG. 1. Expression of H-2 MHC haplotypes in C57BL/6-TgNSE(VSV/Hsp70)5769OGL (*H-2*^{b}) mice crossbred with C57BL/10.D2 (*H-2*^{d}) mice in order to create TG *H-2*^{d} mice that express vesicular stomatitis virus G-tagged hsp70 (VSV-hsp70) in neurons (A to D). Murine lymphocytes were purified from whole blood and stained with fluorescently tagged antibodies recognizing a murine H-2^b (FITC, *x* axis) or H-2^d (PE, *y* axis) MHC class I alloantigen. Staining profiles were then examined by flow cytometry. (A) Unstained control murine lymphocytes. (B) Lymphocytes from a C57BL/6 *H-2*^{b} mouse. (C) Progeny from the F_1 backcross show heterozygous staining for the both *H-2*^{b} and *H-2*^{d} haplotypes. (D) Progeny from the F_2 backcross show homozygous staining for the *H-2*^{d} haplotype. (E) RT-PCR analysis of transgene expression from three NT and three TG mice carrying the *H-2*^{d} haplotype. Total RNA was isolated from whole brain. Negative controls included reaction mixtures containing no template (−) and reaction mixtures lacking RT. The positive control used pT7VSV-hsp70 as a template. The 266-bp amplicon indicated transgene expression in TG but not NT mice. Expression of glyceraldehyde-3-phosphate dehydrogenase (G3PDH) was monitored as a housekeeping control gene.

PBMCs and isolated splenocytes was confirmed at weekly intervals by flow cytometry using monoclonal antibodies specific for CD4$^+$ (L3T4; BD Pharmingen) and CD8$^+$ (Ly-3.2; BD Pharmingen) T cells.

RESULTS

Generation of *H-2*^{d}-TG mice. To generate *H-2*^{d} mice that overexpress the major inducible 70-kDa heat shock protein (hsp70) in neurons, homozygous TG *H-2*^{b} C57BL/6 mice overexpressing hsp70 in neurons [C57BL/6-TgNSE(VSV/Hsp70)5769OGL] were backcrossed for two generations with congenic *H-2*^{d} C57BL/10 mice (C57BL/10.D2/NO1aHsd) (8). PBMCs, isolated from whole blood, were used to monitor the H-2 complex haplotype by flow cytometry (Fig. 1A to D). FITC-labeled monoclonal antibodies recognizing an MHC class I molecule in the H-2^b and H-2^d complex were used to stain PBMCs. Unstained PBMCs were included as a negative control (Fig. 1A). Antibody recognizing the H-2^b alloantigen stained PBMCs from NSE-Hsp70 TG mice (Fig. 1B). Analysis of F_1 progeny revealed dual staining for both the *H-2*^{b} and *H-2*^{d} haplotypes in all mice tested (Fig. 1C). Fifty percent of the F_2 generation stained positive for only the *H-2*^{d} haplotype (Fig. 1D). PCR analysis of genomic DNA isolated from the tail confirmed the presence of the *hsp70* transgene in *H-2*^{d} mice (not shown). Approximately two copies of the transgene were present in H-2^d-positive F_2 progeny based upon Southern blot analysis of genomic DNA, and line C57BL/10.D2-TgNSE(VSV/Hsp70)5769OGL was subsequently maintained as homozygous for the transgene (not shown). Expression of the transgene was confirmed by RT-PCR analysis of total RNA isolated from brain tissue of NT and TG *H-2*^{d} mice (Fig. 1E).

MeV Infection of NT and TG *H-2*^{d} mice. Neonatal NT (n = 20) and TG (n = 23) *H-2*^{d} mice were inoculated intracranially in the left cerebral hemisphere with 4×10^4 50% tissue culture infectious doses ($TCID_{50}$) of Ed MeV. For survival analyses, animals were monitored daily over a 28-day time course. Pilot studies showed that virus-induced mortality is not observed after 28 days p.i., consistent with previous findings with *H-2*^{b} mice (8). A weight of <30 to 50% of the mean litter body weight, corresponding to the early-removal criteria, was the best indicator of impending death and was typically associated with dehydration, social withdrawal, and seizure activity. Kaplan-Meier survival curves, censored for early removal of moribund animals, were plotted. Wilcoxon and log-rank tests were used to screen for potential differences in survival between treatment groups, with more-stringent and -definitive analyses performed using the Cox proportional hazards model.

The first death in the Ed MeV-infected NT *H-2*^{d} mice occurred at 14 days p.i. and the last at 24 days p.i., with an overall mortality of 35% (Fig. 2A). Although the mortality is higher than the 15.1% previously reported for Ed MeV-infected NT *H-2*^{b} mice (n = 53) (8), the difference was not statistically significant (P = 0.076). Control mice receiving either uninfected Vero cell lysate or UV-inactivated virus exhibited no neurological abnormalities or mortality (not shown). NT *H-2*^{d} mice were 9.4 times more likely to die than TG *H-2*^{d} mice infected with Ed MeV, where no mortality was observed, and the difference was statistically significant ($P < 0.036$). This result is in contrast to previous results with *H-2*^{b} mice, where hsp70 overexpression promoted MeV gene expression and neurovirulence of Ed MeV (8).

NT *H-2*^{d} mice were infected with Ed N-522D to determine whether the host protection seen in TG *H-2*^{d} mice requires a viral transcriptional response to elevated hsp70. Ed N-522D-infected NT *H-2*^{d} mice did not exhibit a statistically significant difference in the probability of dying from that of NT *H-2*^{d} mice infected with parental Ed MeV (P = 0.344) (Fig. 2). Ed N-522D-infected TG *H-2*^{d} mice had a 2.4 times lesser probability of death than did Ed N-522D-infected NT *H-2*^{d} mice, although this difference also was not statistically significant (P = 0.319) (Fig. 2B). The difference in the probability of death between Ed N-522D-infected TG *H-2*^{d} mice and Ed MeV-infected NT *H-2*^{d} mice was 4.3-fold. This difference approached but did not achieve significance (P = 0.069). Collectively, these mortality data suggested a trend toward protection by hsp70 in *H-2*^{d} mice infected with the N-522D virus, but complete and statistically defensible protection from virus-in-

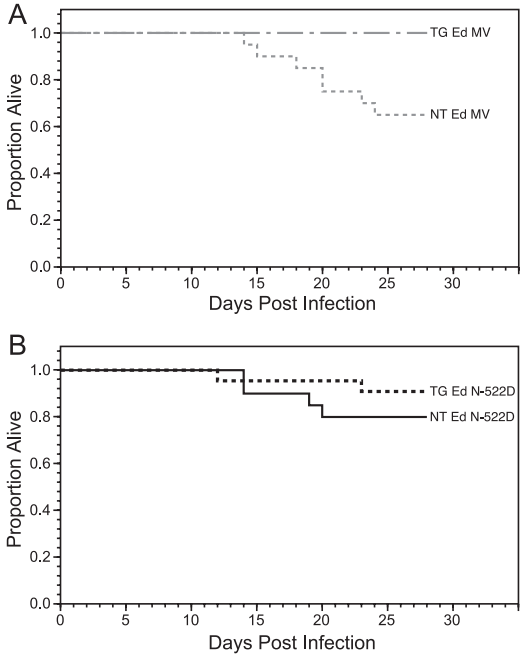

FIG. 2. Survival curves for Ed MeV-infected NT ($n = 20$) and TG ($n = 23$) *H-2*^{d} mice (A) or Ed N-522D-infected NT ($n = 20$) and TG ($n = 22$) *H-2*^{d} mice (B). Kaplan-Meier statistics were used to generate the survival curves. The Wilcoxon and log-rank tests of survival indicated that survival curves differed significantly among the groups. The Cox proportional hazards models further revealed that survival significantly decreased for Ed MeV-infected NT mice relative to that for TG mice ($P < 0.036$). Survival rates of Ed N-522D-infected NT and TG mice did not differ significantly from one other.

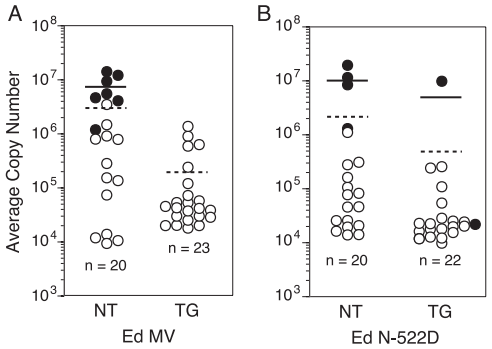

FIG. 3. Viral RNA burden in total brain RNA of Ed MeV-infected (A) or Ed N-522D-infected (B) NT or TG *H-2*^{d} mice. The mean viral RNA copy number in 250 ng of total brain RNA was based on real-time RT-PCR analysis of MeV N gene RNA. In vitro-transcribed N gene RNAs were used as standards. The sensitivity of the assay was ≥100 copies. All samples were run in duplicate, and each result is expressed as a mean. Closed circles represent values derived from moribund animals, whereas open circles represent values from mice that were clinically normal at 28 days p.i. Solid bars represent the mean viral RNA burden of moribund animals, whereas dashed lines represent the mean viral RNA burden for the entire group. No signal was detected in brain RNA harvested from mice inoculated with tissue culture supernatant or UV-inactivated virus (not shown). Differences in mean viral RNA burdens between NT and TG Ed MeV-infected *H-2*^{d} mice (A) were statistically significant ($P < 0.01$, ANOVA). Differences in mean viral RNA burdens between NT and TG Ed N-522D-infected *H-2*^{d} mice (B) did not differ significantly.

duced mortality required both hsp70 overexpression and virus that was capable of mounting a transcriptional response to hsp70 (i.e., Ed MeV).

Mortality was directly correlated to the mean viral RNA burden in the brain. Total RNA was isolated from brains of moribund animals during the acute phase of infection and of animals surviving to 28 days p.i. Quantitative real-time RT-PCR analysis of the viral N-gene sequence was used to calculate the mean viral RNA burden. The lack of mortality seen in Ed MeV-infected TG *H-2*^{d} mice was associated with a 15-fold decrease in the brain viral RNA burden relative to that of Ed MeV-infected NT *H-2*^{d} mice (Fig. 3A). The mean viral RNA burden (per 250 ng of total brain RNA) was $(1.9 \pm 3.4) \times 10^5$ copies for TG *H-2*^{d} animals ($n = 23$) and $(2.9 \pm 4.2) \times 10^6$ copies for NT animals ($n = 20$), a statistically significant difference ($P < 0.01$, one-way analysis of variance [ANOVA]). Within the NT group of animals, there was a strong correlation between mortality and the viral RNA burden. This group consisted of 7 moribund animals and 13 animals that survived to 28 days p.i. The mean viral RNA burden of moribund animals was $(7.2 \pm 4.6) \times 10^6$ copies per 250 ng/total RNA.

The mean brain viral RNA burden for NT *H-2*^{d} mice ($n = 20$) infected with Ed N-522D was $(2.2 \pm 5.1) \times 10^6$ copies per 250 ng total brain RNA, being comparable to that of NT mice infected with Ed MeV (i.e., 2.9×10^6 copies) (Fig. 3B). The burden in TG *H-2*^{d} mice ($n = 22$) infected with Ed N-522D virus was less at $(4.1 \pm 2.1) \times 10^5$. This difference between NT and TG Ed N-522D-infected mice was not statistically significant ($P > 0.05$, one-way ANOVA), although the decreased mean viral RNA burden in the TG Ed N-522D-infected mice was statistically significantly less than that of the NT Ed MeV-infected mice ($P < 0.001$). The latter corresponded to a difference in the probability of mortality that approached but did not achieve statistical significance. As with Ed MeV-infected animals, there was overall correlation between a high brain viral RNA burden and mortality, with five of the six mortalities exhibiting the greatest brain viral RNA burdens. Statistical analysis confirmed the significance of the correlation between survival times and viral burdens. For TG and NT *H-2*^{d} mice infected with either Ed MeV or the Ed N-522D variant, the correlation coefficient was negative and highly significant ($r = 0.833$; $P < 0.0001$). That is, as the viral burden increases, the survival time decreases.

MeV-induced mortality and a high brain viral RNA burden were correlated to increased CPE, which was documented in formalin-fixed paraffin-embedded tissue sections. The brain viral RNA burden was previously correlated to CPE in Ed MeV-infected heat-shocked and nonshocked BALB/c mice (7). The brain viral RNA burden was also correlated to CPE and mortality in NT and TG hsp70-overexpressing *H-2*^{b} mice, where a high brain viral RNA burden was associated with viral RNA-positive cells that formed intranuclear inclusion bodies, expressed the H glycoprotein, and formed syncytia in the hippocampus (8). The present study focused upon Ed MeV-infected TG and NT mice since the mortality and viral RNA burdens were statistically significantly different between these groups of mice.

The majority of both Ed MeV-infected TG ($n = 22/23$) and

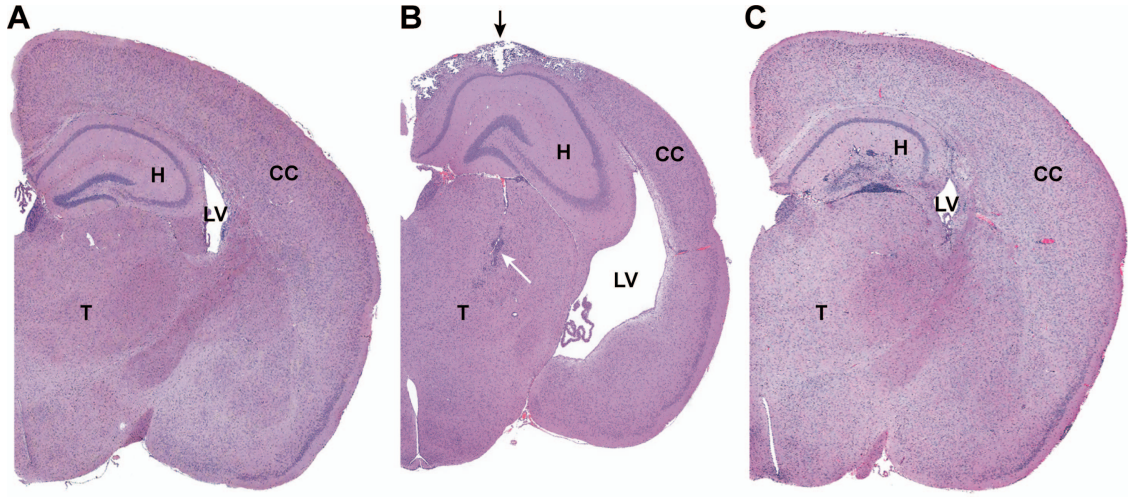

FIG. 4. Brain from sham-inoculated TG (A) or Ed MeV-infected TG (B) or NT (C) mice, harvested at 28 days p.i. Hydrocephalus in Ed MeV-infected TG mice was associated with a reduction in cerebral cortical (CC) thickness by more than 25%, resulting in the enlargement of the lateral ventricles (LV), whereas hydrocephalic changes were not observed in NT Ed MeV-infected mice surviving to 28 days p.i. These subgross images illustrate the paucity of changes in the hippocampus (H) of TG mice even when there is extensive pannecrosis with mineralization in the overlying cerebral cortex (black arrow) and inflammatory infiltrates (white arrow) of the thalamus (T). Findings for TG mice are contrasted to the more pronounced inflammatory involvement of the hippocampus in an NT mouse, where the degree of involvement of the cerebrum and thalamus is not appreciated at this magnification. The latter brain is from the same animal illustrated in Fig. 5C and D. Sham-inoculated control mice lack microscopic lesions.

NT ($n = 20/20$) mice showed evidence of cortical virus-induced CPE, suggesting that the initiation of virus infection within this tissue compartment was not affected by hsp70 overexpression. Tissue changes consisted of leptomeningeal and gray-matter perivascular $CD3^+$ lymphocytic infiltrates, infiltration of the neuropil by lymphocytes, and reactive gliosis in the neuropil (i.e., nonsuppurative meningopolioencephalitis). Selective neuronal cell death was present in Ed MeV-infected NT mice that were moribund between 12 and 24 days p.i. and was characterized by hypereosinophilia and karyorrhexis or karyolysis based upon H&E staining. The majority of dead cells lacked immunohistochemical reactivity for activated caspase 3 (not shown), suggesting that necrosis rather than apoptosis was the predominant basis for cell death, and a progression from selective to pannecrosis was frequently observed. Active neuronal death was not observed at the end of the 28-day-p.i. interval, although areas of previous selective or pannecrosis were marked by foci of mineralization (positive von Kossa histochemical staining), formation of GFAP-positive glial nodules, or tissue loss. These mineralized foci were also evident in Ed MeV-infected TG mice (Fig. 4B), although the incidence was lower, being 30% (7/23), compared to 55% (11/20) for NT mice. Inflammatory infiltrates or other pathological changes were not observed at 28 days p.i. with saline or UV-inactivated virus.

Mortality in Ed MeV-infected NT *H-2*^{d} mice was correlated to virus-induced neuronal cell death in the CA1 to -3 layers of the hippocampus and the granular cell layer of the dentate gyrus, with the greatest severity of change being present in CA2 and -3 neuronal populations. During the acute phase of infection (i.e., prior to 28 days p.i.), neuronal syncytium formation was observed. Syncytia exhibited a progression to cell death, reactive gliosis, and mineralization. As in the cortex, the majority of dead neurons lacked immunoreactivity for activated caspase 3. These changes were associated with $CD3^+$ lymphocytic inflammatory infiltrates. Acute changes in the hippocampus are illustrated in later sections of this article, where affects of T-cell depletion are described (see below). For animals surviving to 28 days p.i., neuronal death was evidenced by neuronal dropout, foci of mineralization, and GFAP-positive glial nodules, and the magnitude of inflammation was increased. Representative changes are illustrated in Fig. 4 and 5). The incidence of reactive glial and inflammatory changes was proportionate to the magnitude of neuronal death, with 55% (11/20) of the NT-infected mice exhibiting hippocampal neuronal death and 80% (16/20) exhibiting hippocampal glial and/or inflammatory responses. Of the animals exhibiting neuronal death, the incidence was 80% in the acute mortality group and 40% in the survivors. In contrast, evidence of hippocampal neuronal death was 22% (5/23) in Ed MeV-infected TG mice (i.e., less than half of that observed in NT mice), and the overall incidence of inflammatory/glial responses was 48% (11/23).

Decreased mortality of Ed MeV-infected TG mice was associated with an increased incidence of hydrocephalus ex vacuo. The change was characterized by a bilateral reduction in cerebrocortical thickness by greater than 25% and an expanded volume of the lateral ventricles (i.e., hydrocephalus) (Fig. 4). The third and fourth ventricles were normal in size, there was no cranial deformation (i.e., macrocephaly), and the amount of cerebrospinal fluid within the subarachnoid space was within normal limits. These changes are consistent with ventricular enlargement secondary to a loss of periventricular tissues (i.e., hydrocephalus ex vacuo), as has previously been described in association with immune-mediated clearance of Sindbis virus from brains of C57BL/6 mice (24). The incidence of hydrocephalus was 35% (8/23) in TG mice, whereas no hydrocephalus was observed in the MeV-infected NT group

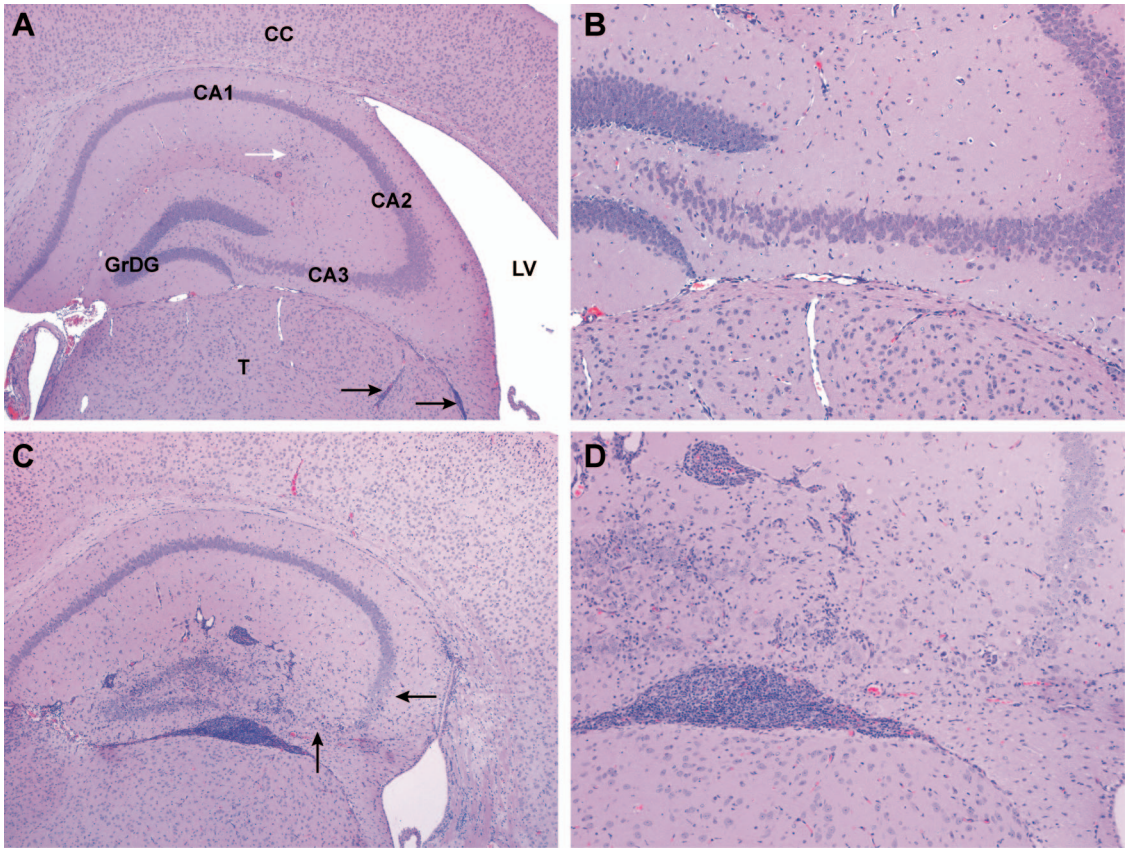

FIG. 5. Representative pathological anatomical changes in brains of TG (A and B) or NT (C and D) mice at 28 days following intracranial inoculation with Ed MeV. Sections illustrate the hippocampal and dentate gyrus and the adjacent thalamus (T), lateral ventricle (LV), and cerebral cortex (CC), shown here in H&E-stained sections of formalin-fixed tissues at magnification ×4 (A and C) or ×10 (B and D). Granular cell neurons of the dentate gyrus (GrDG) and pyramidal neurons of the CA1, CA2, and CA3 regions of the hippocampus were unaffected in 78% of the TG mice, as shown in panels A and B, where minimal leptomeningeal inflammatory infiltrates (black arrows) and a region of minimal hippocampal gliosis (white arrow) were the only significant findings within these structures. The field illustrated in panel B lacks significant lesions and is indistinguishable from tissue from sham-inoculated controls. The enlarged lateral ventricle is evidence of hydrocephalus, a change observed in 35% of the Ed MeV-infected TG mice. In contrast, pronounced inflammatory and glial responses involving the hippocampal and dentate gyrus were observed in 80% of the NT mice, and there was evidence of pyramidal neuronal necrosis in 56%, illustrated here as a marked reduction in neuronal density in the CA3 region and a moderate reduction in the CA2 region (arrows) (C and D).

($n = 20$) or within the mock-infected or uninfected TG controls ($n = 5$). This difference between TG and NT mice was statistically significant ($P = 0.004$, Fisher's exact test). Hydrocephalus was sporadically observed in the maintenance C57BL/10.D2-TgNSE(VSV/Hsp70)5769OGL line, consistent with the 4 to 6% incidence reported for C57BL mice (33), although no differences in incidence have been observed between NT and TG mice.

Depletion of T-cell subsets in *H-2*^{d} mice. We demonstrated (Fig. 2) that *H-2*^{d} mice with overexpression of hsp70 are completely protected against intracranial challenge with Ed MeV relative to NT mice, reflecting a reduction in the brain viral burden. Selective T-cell depletions were subsequently performed to determine the basis for the host protective response to Ed MeV in TG *H-2*^{d} mice.

Splenocytes harvested from uninfected control C57BL/10 *H-2*^{d} mice at 1 to 4 weeks of age were stained with the monoclonal antibody L3T4 or Ly-3.2 and analyzed by flow cytometry. The L3T4 antibody recognizes the CD4 molecule and Ly-3.2 recognizes the CD8 molecule on T cells. Compared to those of weanling animals (≥3 weeks of age), spleens of suckling mice (<3 weeks of age) contained fewer CD4$^+$ and CD8$^+$ lymphocytes, although the differences for each subset were less than twofold and did not reach statistical significance (Table 1). Additionally, the CD4-to-CD8 cell ratio in the developing spleen (1.2 to 1.0, average for weeks 1 and 2) did not statistically differ from that observed in the weanling spleen (1.6 to 1.0, average for weeks 3 and 4). For T-cell depletion, suckling mice were inoculated twice weekly for 4 weeks with 0.1 mg/kg of body weight of anti-CD4 (GK1.5) or anti-CD8 (2.43) monoclonal antibody. Antibodies selectively depleted the corresponding T-cell subset during the 28-day time course (Table 1). Treatment of animals with the combined GK1.5 and 2.43 monoclonal antibodies resulted in complete CD4$^+$ and CD8$^+$ T-cell depletion (not shown). Depletion of T cells was also monitored in PBMCs collected from whole blood at the time of sampling, and complete depletion of the respective T-cell subset was confirmed (not shown).

With the utility of the approach to T-cell depletion established, CD4$^+$ and/or CD8$^+$ T cells were depleted in neonatal

TABLE 1. Percentage of $CD4^+$ or $CD8^+$ T cells in H-2^d mice following weekly administration of anti-mouse CD4 (GK1.5) or CD8 (2.43) monoclonal antibody[a]

Time point	% T cells in indicated subset with or without antibody treatment			
	$CD4^+$		$CD8^+$	
	No treatment	Anti-CD4	No treatment	Anti-CD8
wk 1	15.1	0.2	12.9	0.1
wk 2	13.5	0.1	11.0	0.1
wk 3	23.5	0.2	13.3	0.1
wk 4	23.6	0.1	16.6	0.2

[a] Values represent a percentage of the total number of splenocytes that were counted, are an average for two animals per group, and were detected with monoclonal antibodies distinct from those used for the depletion; $CD4^+$ T cells were labeled with antibody L3T4, and $CD8^+$ T cells were labeled with antibody Ly-3.2. Levels of $CD4^+$ T cells were not affected by the administration of anti-CD8 antibody and vice versa (not shown).

NT and TG *H-2*^{d} mice at the time of intracranial challenge with Ed MeV. Mortality in $CD4^+$ T-cell-depleted NT mice ($n = 18$) was 94%, compared to 63% in $CD8^+$ T-cell depleted NT mice ($n = 16$) (Fig. 6A). Survival analysis revealed that CD4-depleted mice were three times more likely to die than CD8-depleted mice ($P < 0.009$), showing that $CD4^+$ T cells are essential for protection against Ed MeV in NT mice. This result is consistent with findings of previous studies with BALB/c (*H-2*^{d}) mice (15). In contrast, $CD4^+$ T-cell-depleted TG *H-2*^{d} mice ($n = 17$) were only 1.7 times more likely to die than $CD8^+$ T-cell-depleted TG *H-2*^{d} mice ($n = 15$), a difference that was not statistically significant (Fig. 6B). Mortality in TG *H-2*^{d} animals was 41% for CD4-depleted mice and 27% for CD8-depleted mice. This result shows that hsp70-overexpressing *H-2*^{d} mice are less reliant on $CD4^+$ and $CD8^+$ T cells for protection than NT mice. With a combined $CD4^+/CD8^+$ T-cell depletion in TG *H-2*^{d} mice, mortality following Ed MeV infection ($n = 15$) was only 73%, approximating the additive effect of depleting $CD4^+$ (41%) and $CD8^+$ (27%) T cells individually (Fig. 6B). Mice with combined CD4/$CD8^+$ T-cell depletion were three times ($P < 0.02$) and five times ($P < 0.005$) more likely to die than $CD4^+$ or $CD8^+$ T-cell-depleted mice, respectively. The inability to achieve greater than 73% mortality in TG *H-2*^{d} mice, even after depletion of both $CD4^+$ and $CD8^+$ T cells, suggests that overexpression of hsp70 confers a level of innate immunity that contributes to decreased virus-induced mortality.

Histological analysis of T-cell-depleted TG mice confirmed the efficacy of the depletion protocol in that no $CD3^+$ cells were observed within brain sections representing either the acute or chronic phase of infection. Infiltrates were observed following $CD8^+$ T-cell depletion but were minimal when $CD4^+$ T cells were depleted and were absent when both $CD4^+$ and $CD8^+$ T cells were depleted. The increase in mortality that was observed with the combined T-cell depletion was associated with an increase in the viral CPE within the hippocampus, providing further support for the association between hippocampal lesions and virus-induced mortality. The incidence of neuronal death was 38% (5/13 mice examined histologically) in Ed MeV TG mice in which T cells were depleted. Neurons in the CA1 to -3 layers of the hippocampus and the granular cell layer of the dentate gyrus exhibited intranuclear and cytoplasmic inclusion body formation, in addition to syncytium formation and selective neuronal death (Fig. 7). These changes are consistent with previous findings for hsp70-overexpressing *H-2*^{b} C57BL/6 mice (8) and parallel pathological findings for human measles inclusion body encephalitis (12, 13, 16).

Depletion of T cells did not significantly influence the incidence of hydrocephalus in TG mice. The incidence, based upon the number of animals available for histological analysis, was 36% (5/14) for $CD4^+$ T-cell-depleted TG mice, 27% (4/15) for $CD8^+$ T-cell-depleted TG mice, and 15% (2/13) for TG mice in which both $CD4^+$ and $CD8^+$ T cells were depleted. These differences were not statistically significant. For all cases of hydrocephalus in TG mice ($n = 19$), the majority (17/19) were observed in animals surviving to 28 days p.i. None of the T-cell-depleted NT mice exhibited hydrocephalus, from a total of 27 animals examined histologically. Results suggest that innate responses to viral infection contribute to the develop-

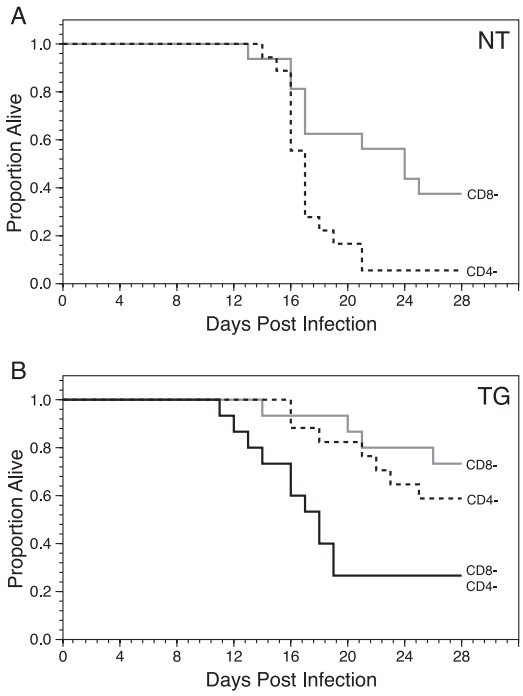

FIG. 6. Effect of selective T-cell depletion on survival of NT (A) or TG (B) *H-2*^{d} mice challenged intracranially with Ed MeV. The NT animals were treated with monoclonal antibodies to deplete either $CD4^+$ T cells ($n = 18$) or $CD8^+$ T cells ($n = 16$) at the time of infection and at weekly intervals thereafter. Kaplan-Meier statistics were used to generate the survival curves, and all mice were censored on day 28 p.i. The Cox proportional hazards models indicated that survival was significantly decreased in $CD4^+$ T-cell-depleted NT mice relative to that for $CD8^+$ T-cell-depleted NT mice challenged with Ed MeV ($P < 0.009$). (B) Survival of TG *H-2*^{d} mice challenged intracranially with Ed MeV and treated with monoclonal antibodies specific for either $CD4^+$ T cells ($n = 17$), $CD8^+$ T cells ($n = 15$), or a mixture of monoclonal antibodies specific for both T-cell subsets ($n = 15$). The Cox proportional hazards models indicated that survival was not significantly different for mice in which $CD4^+$ T cells versus $CD8^+$ T cells were depleted. Combined depletion of $CD4^+$ and $CD8^+$ T cells in TG mice resulted in mortality that remained less than that of $CD4^+$ T-cell-depleted NT mice (73% versus 94%, respectively).

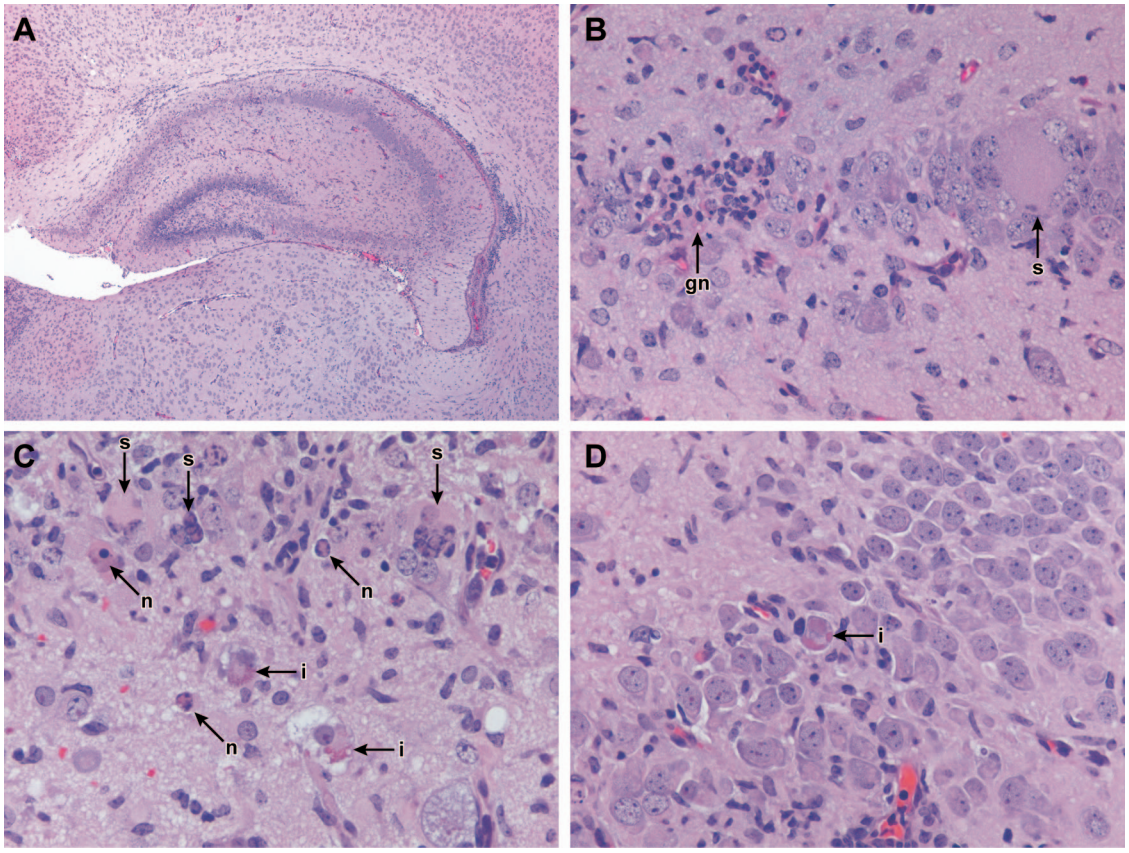

FIG. 7. Depletion of T cells in TG mice caused increased mortality between 11 and 19 days p.i. that was associated with viral CPE and reactive gliosis in the dentate and hippocampal gyrus. Lymphocytic infiltrates were absent in mice in which both $CD4^+$ and $CD8^+$ T cells were depleted, shown here in H&E-stained sections of formalin-fixed tissues at magnification ×4 (A) or ×40 (B). Pyramidal neurons of the hippocampus (B) exhibited syncytium formation (s) that progressed to neuronal death with formation of reactive microglial nodules (gn). These changes were identical to those observed in the acute deaths of NT mice independent of T-cell depletion. CPEs unique to T-cell-depleted TG mice were the formation of neuronal inclusion bodies and the formation of granular cell neuron syncytia. Panel C is a ×50 magnification illustrating these CPEs in both granular cell neurons (upper half) and sporadic pyramidal neurons (midlevel). Individualized neuronal death characterized by hypereosinophilic soma was interpreted as necrosis (n) based upon lack of immunohistochemical reactivity to activated caspase 3 (not shown), and this change accompanied the formation of syncytia. Dead cells often exhibited nuclear hypereosinophilia associated with margination of chromatin along the nuclear membrane, compatible with Cowdry type B paramyxovirus intranuclear inclusions. Eosinophilic cytoplasmic inclusion bodies were observed in pyramidal neurons (i), shown here in two cells undergoing vacuolar degeneration. Sporadic pyramidal neurons exhibited both eosinophilic cytoplasmic and intranuclear Cowdry type B inclusions (D).

ment of hydrocephalus and host protection in hsp70-overexpressing TG mice.

Innate immune responses in infected mice. Total brain RNA was analyzed by real-time RT-PCR in order to provide direct evidence for enhanced innate immune responses in infected TG mice relative to those in NT mice. Sampling was designed to precede virus-induced mortality, which occurs as early as 11 days p.i., and to precede the onset of adaptive immune responses, previously shown to be detectable by 14 days p.i. based upon MeV-specific splenocyte blastogenic responsiveness (7). Accordingly, mice were inoculated via the intracranial route with 4×10^4 $TCID_{50}$ Ed MeV as described above, together with sham-inoculated controls, and brains were harvested at 5 and 10 days p.i. Each time point was represented by five infected and two uninfected TG or NT mice.

Mononuclear inflammatory cell infiltrates of the brain were observed at 10 but not 5 days p.i. based upon evaluation of H&E-stained frozen sections, and these infiltrates exhibited CD4 but not CD8 immunoreactivity (not shown). Infiltrates were present in the leptomeninges, cerebral cortices, and hippocampus and with no apparent differences in the distribution or magnitude of the response between TG and NT mice. The RNA analyses thus focused on the 5-day-p.i. time point in order to maximize representation of intrinsic tissue responses to viral challenge.

Expression of CD68 and that of MHC II mRNAs were used as markers of innate immune activation, with CD68 and MHC II being expressed by activated microglial/macrophages and MHC II also being expressed by activated astrocytes and endothelial cells (26). Levels of transcript that were measured by real-time RT-PCR were significantly greater for TG mice than for NT mice for both CD68 and MHC II ($P < 0.05$, ANOVA) (Fig. 8). hsp70 can stimulate innate immune responses in the central nervous system (CNS) through interaction with TLRs, specifically TLR2 and TLR4 (1, 21). We therefore examined

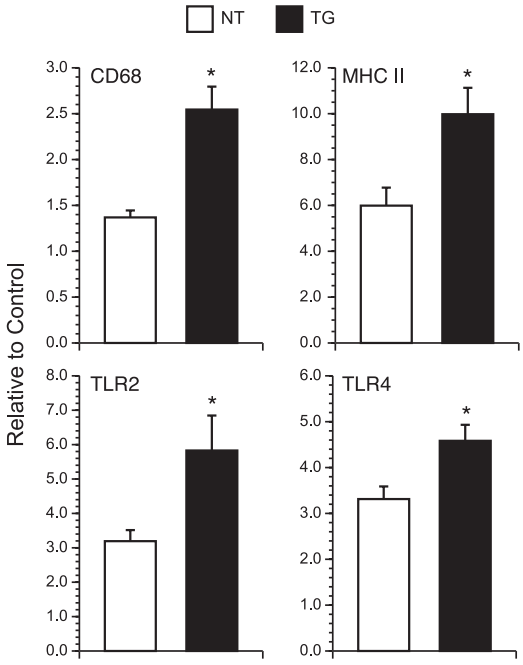

FIG. 8. Transcript levels for CD68, MHC II, TLR2, and TLR4 in total brain RNA of infected and sham-infected control NT and TG mice. Samples were collected at 5 days p.i. The RNA was analyzed by real-time RT-PCR, adjusted for 18S RNA levels, and results from infected mice expressed as *n*-fold changes relative to the basal expression that was detected in the corresponding uninfected control group. Results are expressed as means ± standard errors of the means. Statistically significant differences ($P < 0.05$, ANOVA) are represented by asterisks.

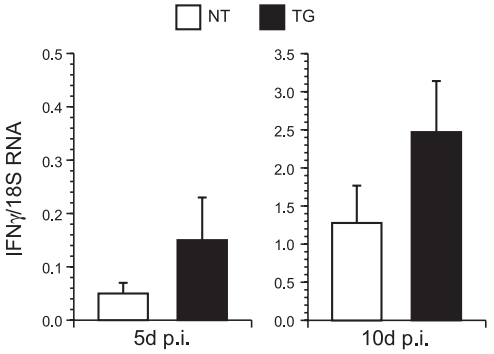

FIG. 9. Transcript levels of IFN-γ in total brain RNA of infected and sham-infected control NT and TG mice at 5 and 10 days p.i. The RNA was analyzed by real-time RT-PCR and adjusted for 18S RNA levels. Significant levels of transcripts were not detected in uninfected controls (not shown). Results are expressed as means ± standard errors of the means.

TLR2 and TLR4 transcript expression as evidence of signaling through these pathways. Transcripts for both TLRs were significantly elevated in brains of infected TG mice relative to levels for infected NT controls ($P < 0.05$, ANOVA) (Fig. 8).

Activated microglia/macrophages are a potent source of IFN-γ (23, 54), and this cytokine is known to mediate noncytolytic clearance of MeV from the brain (44). We therefore measured IFN-γ transcript levels within total RNA from infected brain tissues by real-time RT-PCR. Transcript levels were increased approximately threefold for infected TG mice relative to levels for infected NT mice, although differences were not statistically significant due to a large standard deviation of the mean (Fig. 9). Transcripts from 10 days p.i. were examined to determine if differences might be amplified by infiltrating T cells. The TG-infected mice exhibited an approximately twofold increase in IFN-γ transcript levels relative to those for NT-infected mice, but again the difference was not statistically significant due to a large standard deviation of the mean. This result indicates that IFN-γ production alone does not explain the enhanced protection against MeV challenge that is mediated by hsp70.

DISCUSSION

Results of the current study show that selective neuronal overexpression of hsp70 in *H-2*^{d} C57BL/6 mice can reduce the brain viral RNA burden, reduce virus-induced CPE in the hippocampus, and eliminate virus-induced mortality. These results are similar to those of previous work with *H-2*^{d} BALB/c mice where hsp70 was elevated by transient whole-body hyperthermia prior to intracranial Ed MeV inoculation (7). The mean Ed MeV RNA burden for TG *H-2*^{d} C57BL/10 mice was 15 times lower than that observed for NT mice. The protective effects of hsp70 overexpression remained apparent when both $CD4^+$ and $CD8^+$ T cells were depleted, indicating an hsp70-dependent enhancement of innate immunity. Enhanced innate immunity was directly supported by the increased expression of markers of innate immune activation (i.e., CD68 and MHC II transcript levels), as well as the expression of transcripts for TLR2 and TLR4, well-established mediators of innate immune activation in cells such as microglia and macrophages. Enhanced microglial/macrophage activation in brain following TLR activation is associated with a number of responses that could promote antiviral immunity, including production of cytokines with direct antiviral activity (e.g., IFN-γ [23, 54]). The effector cytokines and/or chemokines relevant to hsp70-mediated protection remain to be established and may be multiple. While the observed increase in IFN-γ production for infected TG mice relative to that for infected NT mice was not statistically significant in the present work, we cannot exclude its relevance. Cytokine and chemokine networks act synergistically, amplifying the host protective role of any one component.

TLRs differ in the type of ligand that they recognize (i.e., exogenous versus endogenous) and in the intracellular versus extracellular location of these recognition events. TLR2 and -4 are unique in that they recognize extracellular endogenous ligands, such as heat shock proteins, and extracellular hsp70 is known to activate microglia/macrophages predominantly through TLR4 but also through TLR2 (21). Stimulation of TLR4 by hsp70 results in secretion of IFN-γ, nitric oxide, tumor necrosis factor alpha, interleukin 1β, interleukin 6, CCL2 to -5, and CXCL1 (5, 46, 49). In order to engage these TLRs, hsp70 would need to be released from cells, and this could occur either through secretory mechanisms or following cell death due to viral CPE. The latter would be maximal for virus mounting a transcriptional response to hsp70, and this

may explain why complete protection against virus-induced mortality was observed in TG mice infected with Ed MeV but not the N-522D variant. In previous work, infected *H-2*^{b} TG mice show enhanced transcript levels for Ed MeV but not Ed N522D virus relative to those for infected NT controls, establishing the in vivo relevance of in vitro studies showing loss of viral transcriptional responsiveness to hsp70 when the Ed N protein amino acid 522 is changed from asparagine to aspartic acid (8). The extracellular release of hsp70 in response to viral infection has been shown for parvovirus H1 (32), and the extracellular release of hsp70 in the CNS has recently been documented as part of the inflammatory responses to ischemia-reperfusion injury (2). The extracellular release of hsp70 emerges as a probable link between the virus-infected cell and the uninfected cells that are primarily responsible for initiating innate and adaptive immune responses. Recognition of the dual role of hsp70 as an intracellular chaperone and extracellular cytokine is the basis for the term "chaperokine".

Two aspects of models of virus-hsp70 interaction should be emphasized. First, the mouse model used for the current study is less permissive to MeV infection than are the MeV receptor TG lines (i.e., lines expressing human CD46 or CD150). It is possible that in a more permissive system, a host-protective effect of hsp70 may be demonstrable independently of the viral transcriptional response. This possibility is supported by the tendency toward host protection (albeit not statistically significant) in *H-2*^{d} TG mice infected with the Ed N-522D virus. Second, the hemagglutinin protein of wild-type strains (but not that of the Ed MeV strain used in the current study) has been reported to activate TLR2 signaling in vitro, raising the possibility that viral proteins contribute to extracellular TLR signaling by hsp70 (3).

Enhanced immune activation within infected TG mice does appear to have a cost—cerebral cortical atrophy resulting in secondary enlargement of the lateral ventricles. In the mouse model of brain infection by Sindbis virus, viral clearance by $CD4^+$ T cells and microglia/macrophages is associated with tissue loss that results in enlargement of the lateral ventricles (24). This specific type of lateral ventricular enlargement is known as hydrocephalus ex vacuo and is contrasted with obstructive hydrocephalus, in which an impaired flow of cerebrospinal fluid causes increased intracranial pressure, resulting in enlargement of the calvarium in neonates and cerebral cortical atrophy. Obstructive hydrocephalus has been found in MeV-infected hamsters (18), where glial scarring in the mesencephalic aqueduct follows ependymal infection, but results of the current work lack evidence of the ependymal infection and enlargement of the third ventricle that should accompany stricture of the mesencephalic aqueduct. A role for hsp70-mediated activation of innate immune responses as a cause for hydrocephalus in the current work is supported by the fact that depletion of T-cell subsets fails to significantly reduce the increased incidence of hydrocephalus that is observed in infected TG mice. The benefit of minimizing virus-induced CPE in the hippocampus offsets the cost of cerebral cortical atrophy in infected TG mice. Mounting evidence suggests that hippocampal injury is a basis for sudden death in humans (48).

A central role for microglia and/or bone marrow-derived macrophages in mediating hsp70-mediated outcomes of MeV infection can be used to reconcile the *H-2* haplotype-dependent differences in the outcome of MeV-hsp70 interaction in brain. In an *H-2*^{b} background, the host immune system cannot exploit (or contain) the hsp70-dependent stimulation of viral gene expression, and the result is an unchecked viral spread and increase in viral CPE and virus-induced mortality. In contrast, the viral transcriptional responsiveness to hsp70 is exploited in *H-2*^{d} mice to enhance antiviral immune mechanisms that ultimately reduce the brain viral RNA burden and eliminate virus-induced mortality. Others have shown that cytokine production is altered in monocytes and T cells of *H-2*^{b} mice relative to that for congenic *H-2*^{d} mice (28, 29), and we propose that microglia and monocyte-derived macrophages may respond differently to hsp70 ligands as a function of the *H-2* allele. Cytokine and chemokine responses of mouse microglia also differ as a function of age. Responses are reduced in microglia recovered from neonatal mice relative to those for weanling mice, leading Schell et al. (46) to propose that microglial responsiveness to TLR ligands may serve as a basis for the age-dependent differences in the outcome of MeV infection of the brain (i.e., enhanced neonatal susceptibility) (17, 25, 47). In context of our studies, this may explain the comparable susceptibility of neonatal *H-2*^{b} and *H-2*^{d} NT mice to MeV infection. The viral RNA burden is comparable between NT *H-2*^{d} mice and that previously reported for NT *H-2*^{b} mice (i.e., 2.9×10^6 versus 3.5×10^6 copies of viral N gene target per 250 ng total brain RNA), and the 35% mortality rate for infected NT *H-2*^{d} mice is not significantly different from the previously reported 15.1 to 30% mortality rate for *H-2*^{b} mice (8, 45). The differences in susceptibilities of *H-2*^{b} and *H-2*^{d} mice to MeV brain infection that have been described in the literature are based upon intracranial inoculation of weanling mice and not results for neonates (35, 36, 55). Increasing the strength of a microglial activation stimulus, in this case through TG hsp70 overexpression, may thus unmask the *H-2* haplotype-dependent differences in microglial responses to activation stimuli. Future studies must identify components of the innate immune response that are responsible for hsp70-dependent host protection in *H-2*^{d} mice so that we may then define specific deficiencies in the $H\text{-}2^b$ response that underlie enhanced susceptibility to viral infection.

Our understanding of the immune parameters required for protection in MeV infection of humans remains incomplete, although increased expression of hsp70 should be a characteristic feature of infection. hsp70 is both constitutively expressed and inducible in humans, in contrast to the lack of significant basal expression in rodents (7, 34). Fever is a consistent sequela to MeV infection (19), and temperature elevations as low as 39°C are potent inducers of hsp70 in the human brain (34). Heat-shock-induced hsp70 levels are stable in the brain (43), where hsp70 is localized primarily to the soma of neurons (50). The degree to which hsp70 levels in our TG mice approximate basal versus heat-shock-induced levels in humans remains to be established, although any increase in levels of hsp70 in neurons of mice represents a change that more closely approximates results with human tissues. MeV infection of humans is controlled in part by both virus-specific humoral and cell-mediated immune responses, although T cells appear to play a dominant role during primary infection (51). No clear link exists between MHC alleles and T-cell-mediated protection in humans (10, 11); however, several class I alleles have

been associated with MeV-induced IFN-γ secretion (42). MHC class III allelic variation has not been examined in the immune response to MeV infection, although genes in this region encode diverse proteins involved in immune and inflammatory responses. Two genes encoding hsp70 are found in the MHC class III region of humans (31), and hsp70 contributes to MHC class I antigen expression (56), illustrating the fundamental linkage between hsp70 and immune/inflammatory responses.

In conclusion, hsp70-overexpressing *H-2*^{d} mice recapitulate key features of the acute sequela to MeV infection of the human brain. Brain infection is a characteristic feature of MeV infection in humans. Electroencephalographic evidence for CNS invasion has been observed in 50% of uncomplicated cases of naturally occurring MeV infection, and MeV N transcripts have been detected in the brains of 18% of autopsy cases unassociated with MeV-induced neurological disease (6, 22). Despite this frequency of CNS invasion, neurological disease is rare, supporting the effectiveness of antiviral immunity. This infection outcome is modeled by the infected TG mice, and the increased mortality observed in NT infected mice supports a pivotal role for hsp70 in mediating host protection. Immune suppression in TG *H-2*^{d} mice (e.g., T-cell depletion) increases the incidence of a fulminate and highly cytopathic form of CNS infection that exhibits features of measles inclusion body encephalitis, an acute infection outcome observed in immunocompromised humans. The contribution of MHC to outcomes of human brain infection and the ability of TG mice to model a rare and chronic sequela to MeV infection of humans (i.e., subacute sclerosing panencephalitis) remain to be established.

ACKNOWLEDGMENTS

This work was supported by funds from the National Institute of Neurological Disorders and Stroke (R01NS31693). Thomas Carsillo was supported in part by an NIH/NIAID award (T32-AI-065411) administered by the Center for Microbial Interface Biology (CMIB), the Ohio State University.

REFERENCES

1. **Akira, S., and K. Takeda.** 2004. Toll-like receptor signalling. Nat. Rev. Immunol. **4:**499–511.
2. **Awad, H., Z. Suntres, J. Heijmans, D. Smeak, V. Bergdall-Costell, F. L. Christofi, C. Magro, and M. Oglesbee.** 2008. Intracellular and extracellular expression of the major inducible 70kDa heat shock protein in experimental ischemia-reperfusion injury of the spinal cord. Exp. Neurol. **212:**275–284.
3. **Bieback, K., E. Lien, I. M. Klagge, E. Avota, J. Schneider-Schaulies, W. P. Duprex, H. Wagner, C. J. Kirschning, V. ter Meulen, and S. Schneider-Schaulies.** 2002. Hemagglutinin protein of wild-type measles virus activates Toll-like receptor 2 signaling. J. Virol. **76:**8729–8736.
4. **Bourhis, J. M., B. Canard, and S. Longhi.** 2006. Structural disorder within the replicative complex of measles virus: functional implications. Virology **344:**94–110.
5. **Brannan, C. A., and M. R. Roberts.** 2004. Resident microglia from adult mice are refractory to nitric oxide-inducing stimuli due to impaired NOS2 gene expression. Glia **48:**120–131.
6. **Brooks, G. F., J. S. Butel, and S. A. Morse.** 1998. Paramyxovirus and rubella virus, p. 507–527. *In* J. P. Butler, J. Ransom, and E. Ryan (ed.), Adelberg's microbiology. Appleton and Lange, Stamford, CT.
7. **Carsillo, T., M. Carsillo, S. Niewiesk, D. Vasconcelos, and M. Oglesbee.** 2004. Hyperthermic pre-conditioning promotes measles virus clearance from brain in a mouse model of persistent infection. Brain Res. **1004:**73–82.
8. **Carsillo, T., Z. Traylor, C. Choi, S. Niewiesk, and M. Oglesbee.** 2006. Hsp72—a host determinant of measles virus neurovirulence. J. Virol. **80:** 11031–11039.
9. **Carsillo, T., X. Zhang, D. Vasconcelos, S. Niewiesk, and M. Oglesbee.** 2006. A single codon in the nucleocapsid protein C terminus contributes to in vitro and in vivo fitness of Edmonston measles virus. J. Virol. **80:**2904–2912.
10. **Cattaneo, R., G. Rebmann, K. Baczko, V. ter Meulen, and M. A. Billeter.** 1987. Altered ratios of measles virus transcripts in diseased human brains. Virology **160:**523–526.
11. **Cztonkowska, A., M. Klos, and B. Iwinska.** 1986. Lack of relationship between the HLA system and subacute sclerosing panencephalitis. Acta Neurol. Scand. **73:**304–305.
12. **Esiri, M. M., and P. G. Kennedy.** 1997. Viral diseases, p. 3–63. *In* D. I. Graham and P. L. Lantos (ed.), Greenfield's neuropathology. Arnold, New York, NY.
13. **Esiri, M. M., D. R. Oppenheimer, B. Brownell, and M. Haire.** 1982. Distribution of measles antigen and immunoglobulin-containing cells in the CNS in subacute sclerosing panencephalitis (SSPE) and atypical measles encephalitis. J. Neurol. Sci. **53:**29–43.
14. **Finke, D., U. G. Brinckmann, V. ter Meulen, and U. G. Liebert.** 1995. Gamma interferon is a major mediator of antiviral defense in experimental measles virus-induced encephalitis. J. Virol. **69:**5469–5474.
15. **Finke, D., and U. G. Liebert.** 1994. CD4+ T cells are essential in overcoming experimental murine measles encephalitis. Immunology **83:**184–189.
16. **Freeman, A. F., D. A. Jacobsohn, S. T. Shulman, W. J. Bellini, P. Jaggi, G. de Leon, G. F. Keating, F. Kim, L. M. Pachman, M. Kletzel, and R. E. Duerst.** 2004. A new complication of stem cell transplantation: measles inclusion body encephalitis. Pediatrics **114:**e657–e660.
17. **Griffin, D. E., J. Mullinix, O. Narayan, and R. T. Johnson.** 1974. Age dependence of viral expression: comparative pathogenesis of two rodent-adapted strains of measles virus in mice. Infect. Immun. **9:**690–695.
18. **Haspel, M. V., and F. Rapp.** 1975. Measles virus: an unwanted variant causing hydrocephalus. Science **187:**450–451.
19. **Hutchins, S. S., M. J. Papania, R. Amler, E. F. Maes, M. Grabowsky, K. Bromberg, V. Glasglow, T. Speed, W. J. Bellini, and W. A. Orenstein.** 2004. Evaluation of the measles clinical case definition. J. Infect. Dis. **189**(Suppl. 1)**:**S153–S159.
20. **Jones, T. B., D. M. Basso, A. Sodhi, J. Z. Pan, R. P. Hart, R. C. MacCallum, S. Lee, C. C. Whitacre, and P. G. Popovich.** 2002. Pathological CNS autoimmune disease triggered by traumatic spinal cord injury: implications for autoimmune vaccine therapy. J. Neurosci. **22:**2690–2700.
21. **Kakimura, J., Y. Kitamura, K. Takata, M. Umeki, S. Suzuki, K. Shibagaki, T. Taniguchi, Y. Nomura, P. J. Gebicke-Haerter, M. A. Smith, G. Perry, and S. Shimohama.** 2002. Microglial activation and amyloid-beta clearance induced by exogenous heat-shock proteins. FASEB J. **16:**601–603.
22. **Katayama, Y., H. Hotta, A. Nishimura, Y. Tatsuno, and M. Homma.** 1995. Detection of measles virus nucleoprotein mRNA in autopsied brain tissues. J. Gen. Virol. **76:**3201–3204.
23. **Kawanokuchi, J., T. Mizuno, H. Takeuchi, H. Kato, J. Wang, N. Mitsuma, and A. Suzumura.** 2006. Production of interferon-gamma by microglia. Mult. Scler. **12:**558–564.
24. **Kimura, T., and D. E. Griffin.** 2003. Extensive immune-mediated hippocampal damage in mice surviving infection with neuroadapted Sindbis virus. Virology **311:**28–39.
25. **Lawrence, D. M., M. M. Vaughn, A. R. Belman, J. S. Cole, and G. F. Rall.** 1999. Immune response-mediated protection of adult but not neonatal mice from neuron-restricted measles virus infection and central nervous system disease. J. Virol. **73:**1795–1801.
26. **Lemstra, A. W., J. C. Groen in't Woud, J. J. Hoozemans, E. S. van Haastert, A. J. Rozemuller, P. Eikelenboom, and W. A. van Gool.** 2007. Microglia activation in sepsis: a case-control study. J. Neuroinflamm. **4:**4.
27. **Longbrake, E. E., W. Lai, D. P. Ankeny, and P. G. Popovich.** 2007. Characterization and modeling of monocyte-derived macrophages after spinal cord injury. J. Neurochem. **102:**1083–1094.
28. **Matthews, V. B., F. T. Christiansen, and P. Price.** 2000. Lymphocytes from H2 mice produce lower levels of several cytokines than congenic H2 or H2 mice. Immunol. Cell Biol. **78:**247–253.
29. **Matthews, V. B., and P. Price.** 2000. The H2(b) haplotype modifies the production of pro-inflammatory cytokines: implications for immunopathology. Eur. Cytokine Netw. **11:**640–646.
30. **Mayer, M. P.** 2005. Recruitment of Hsp70 chaperones: a crucial part of viral survival strategies. Rev. Physiol. Biochem. Pharmacol. **153:**1–46.
31. **Milner, C. M., and R. D. Campbell.** 1990. Structure and expression of the three MHC-linked HSP70 genes. Immunogenetics **32:**242–251.
32. **Moehler, M., M. Zeidler, J. Schede, J. Rommelaere, P. R. Galle, J. J. Cornelis, and M. Heike.** 2003. Oncolytic parvovirus H1 induces release of heat-shock protein HSP72 in susceptible human tumor cells but may not affect primary immune cells. Cancer Gene Ther. **10:**477–480.
33. **Mori, A.** 1968. Hereditary hydrocephalus in C57BL mouse. Brain Nerve **20:**695–700.
34. **Morrison-Bogorad, M., A. L. Zimmerman, and S. Pardue.** 1995. Heat-shock 70 messenger RNA levels in human brain: correlation with agonal fever. J. Neurochem. **64:**235–246.
35. **Neumeister, C., and S. Niewiesk.** 1998. Recognition of measles virus-infected cells by CD8+ T cells depends on the H-2 molecule. J. Gen. Virol. **79:**2583–2591.
36. **Niewiesk, S., U. Brinckmann, B. Bankamp, S. Sirak, U. G. Liebert, and V. ter Meulen.** 1993. Susceptibility to measles virus-induced encephalitis in mice

correlates with impaired antigen presentation to cytotoxic T lymphocytes. J. Virol. **67:**75–81.
37. **Oglesbee, M.** 2007. Nucleocapsid protein interactions with the major inducible 70 kDa heat shock protein, p. 53–98. *In* S. Longhi (ed.), Measles virus nucleoprotein. Nova Science Publishers, Hauppauge, NY.
38. **Oglesbee, M., S. Ringler, and S. Krakowka.** 1990. Interaction of canine distemper virus nucleocapsid variants with 70K heat-shock proteins. J. Gen. Virol. **71:**1585–1590.
39. **Oglesbee, M. J., H. Kenney, T. Kenney, and S. Krakowka.** 1993. Enhanced production of morbillivirus gene-specific RNAs following induction of the cellular stress response in stable persistent infection. Virology **192:**556–567.
40. **Oglesbee, M. J., Z. Liu, H. Kenney, and C. L. Brooks.** 1996. The highly inducible member of the 70 kDa family of heat shock proteins increases canine distemper virus polymerase activity. J. Gen. Virol. **77:**2125–2135.
41. **Oglesbee, M. J., M. Pratt, and T. Carsillo.** 2002. Role for heat shock proteins in the immune response to measles virus infection. Viral Immunol. **15:**399–416.
42. **Ovsyannikova, I. G., J. E. Ryan, R. A. Vierkant, V. S. Pankratz, R. M. Jacobson, and G. A. Poland.** 2005. Immunologic significance of HLA class I genes in measles virus-specific IFN-gamma and IL-4 cytokine immune responses. Immunogenetics **57:**828–836.
43. **Pardue, S., S. Wang, M. M. Miller, and M. Morrison-Bogorad.** 2007. Elevated levels of inducible heat shock 70 proteins in human brain. Neurobiol. Aging **28:**314–324.
44. **Patterson, C. E., D. M. Lawrence, L. A. Echols, and G. F. Rall.** 2002. Immune-mediated protection from measles virus-induced central nervous system disease is noncytolytic and gamma interferon dependent. J. Virol. **76:**4497–4506.
45. **Sakae, H., M. Kohase, T. Kurata, and H. Yoshikura.** 1997. Isolation of a measles virus variant: protection of newborn mice from measles encephalitis by 24 h prior intracerebral inoculation with the variant. Arch. Virol. **142:** 1937–1952.
46. **Schell, J. B., C. A. Crane, M. F. Smith, Jr., and M. R. Roberts.** 2007. Differential ex vivo nitric oxide production by acutely isolated neonatal and adult microglia. J. Neuroimmunol. **189:**75–87.
47. **Schubert, S., K. Moller-Ehrlich, K. Singethan, S. Wiese, W. P. Duprex, B. K. Rima, S. Niewiesk, and J. Schneider-Schaulies.** 2006. A mouse model of persistent brain infection with recombinant Measles virus. J. Gen. Virol. **87:**2011–2019.
48. **Scorza, F. A., R. M. Cysneiros, R. M. Arida, C. A. Scorza, A. C. de Almeida, B. Schmidt, and E. A. Cavalheiro.** 2008. Adult hippocampal neurogenesis and sudden unexpected death in epilepsy: reality or just an attractive history? Med. Hypotheses **71:**914–922.
49. **Spiller, S., G. Elson, R. Ferstl, S. Dreher, T. Mueller, M. Freudenberg, B. Daubeuf, H. Wagner, and C. J. Kirschning.** 2008. TLR4-induced IFN-gamma production increases TLR2 sensitivity and drives Gram-negative sepsis in mice. J. Exp. Med. **205:**1747–1754.
50. **Tytell, M., W. R. Brown, D. M. Moody, and V. R. Challa.** 1998. Immunohistochemical assessment of constitutive and inducible heat-shock protein 70 and ubiquitin in human cerebellum and caudate nucleus. Mol. Chem. Neuropathol. **35:**97–117.
51. **Uytdehaag, F. G., R. S. van Binnendijk, M. J. Kenter, and A. D. Osterhaus.** 1994. Cytotoxic T lymphocyte responses against measles virus. Curr. Top. Microbiol. Immunol. **189:**151–167.
52. **Vasconcelos, D., E. Norrby, and M. Oglesbee.** 1998. The cellular stress response increases measles virus-induced cytopathic effect. J. Gen. Virol. **79:**1769–1773.
53. **Vasconcelos, D. Y., X. H. Cai, and M. J. Oglesbee.** 1998. Constitutive overexpression of the major inducible 70 kDa heat shock protein mediates large plaque formation by measles virus. J. Gen. Virol. **79:**2239–2247.
54. **Wang, X., and Y. Suzuki.** 2007. Microglia produce IFN-gamma independently from T cells during acute toxoplasmosis in the brain. J. Interferon Cytokine Res. **27:**599–605.
55. **Weidinger, G., S. Czub, C. Neumeister, P. Harriott, V. ter Meulen, and S. Niewiesk.** 2000. Role of CD4(+) and CD8(+) T cells in the prevention of measles virus-induced encephalitis in mice. J. Gen. Virol. **81:**2707–2713.
56. **Wells, A. D., S. K. Rai, M. S. Salvato, H. Band, and M. Malkovsky.** 1998. Hsp72-mediated augmentation of MHC class I surface expression and endogenous antigen presentation. Int. Immunol. **10:**609–617.
57. **Zhang, X., J. M. Bourhis, S. Longhi, T. Carsillo, M. Buccellato, B. Morin, B. Canard, and M. Oglesbee.** 2005. Hsp72 recognizes a P binding motif in the measles virus N protein. Virology **337:**162–174.
58. **Zhang, X., C. Glendening, H. Linke, C. L. Parks, C. Brooks, S. A. Udem, and M. Oglesbee.** 2002. Identification and characterization of a regulatory domain on the carboxyl terminus of the measles virus nucleocapsid protein. J. Virol. **76:**8737–8746.